

Rel-Zero: Harnessing Patch-Pair Invariance for Robust Zero-Watermarking Against AI Editing

Pengzhen Chen^{1,2,3} Yanwei Liu^{1,3†} Xiaoyan Gu^{1,2,3†} Xiaojun Chen^{1,2,3} Wu Liu⁴ Weiping Wang¹

¹Institute of Information Engineering, Chinese Academy of Sciences

²School of Cyber Security, University of Chinese Academy of Sciences

³State Key Laboratory of Cyberspace Security Defense ⁴University of Science and Technology of China

{chenpengzhen, liuyanwei, guxiaoyan, chenxiaojun, wangweiping}@iie.ac.cn, liuwu@ustc.edu.cn

Abstract

Recent advancements in diffusion-based image editing pose a significant threat to the authenticity of digital visual content. Traditional embedding-based watermarking methods often introduce perceptible perturbations to maintain robustness, inevitably compromising visual fidelity. Meanwhile, existing zero-watermarking approaches, typically relying on global image features, struggle to withstand sophisticated manipulations. In this work, we uncover a key observation: while individual image patches undergo substantial alterations during AI-based editing, the relational distance between patch pairs remains relatively invariant. Leveraging this property, we propose Relational Zero-Watermarking (Rel-Zero), a novel framework that requires no modification to the original image but derives a unique zero-watermark from these editing-invariant patch relations. By grounding the watermark in intrinsic structural consistency rather than absolute appearance, Rel-Zero provides a non-invasive yet resilient mechanism for content authentication. Extensive experiments demonstrate that Rel-Zero achieves substantially improved robustness across diverse editing models and manipulations compared to prior zero-watermarking approaches.

1. Introduction

The rapid development of sophisticated generative models, particularly diffusion models [6, 29, 30, 37], has revolutionized digital content creation. Editing frameworks such as InstructPix2Pix [4] and inpainting systems [17, 41] empower users to edit images with unprecedented ease and realism. However, they also raise exigent challenges in content authenticity, copyright protection, and provenance tracking. Digital watermarking serves as a critical technology to address these concerns, yet existing paradigms, embedding watermarking and zero-watermarking, struggle to balance robustness, fidelity, and applicability in the face of

† Corresponding author.

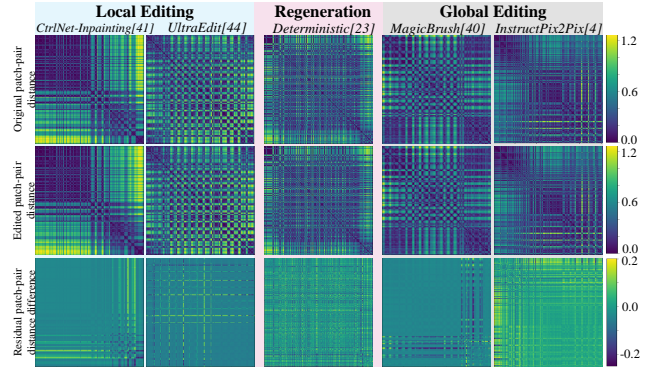


Figure 1. **Analysis of Relational Stability.** We reveal a key insight: Patch-pair distance tends to be preserved after AI editing. This invariant property can be extracted as a zero-watermark. Here we present the patch-pair distance of RGB vectors in original images (first row) and edited images (second row) across five main editing models. The last row illustrates the distance difference between pre-edit and post-edit with a color scale spanning $[-0.2, 0.2]$.

generative edits.

Traditional embedding watermarking paradigms [15, 25, 43, 45] inject watermark signals into the image pixels or frequency domain. To survive aggressive manipulations, especially non-linear generative edits that fundamentally reconstruct pixel data, the embedded signal must be sufficiently strong [5, 14, 24]. This requirement inevitably sacrifices image quality, leading to perceptible artifacts and degradation of the original content. Across domains such as medical imaging [3, 16, 28, 31], autonomous driving [27, 35], and world modeling [2, 9], copyright protection is paramount, yet compromised image fidelity can be catastrophic. The introduction of watermark-induced noise can severely impair the reliability of downstream tasks, which leads to inaccurate diagnosis, deviations in pathological analysis, unstable perception, and distorted environment prediction, ultimately limiting the trustworthiness of high-level visual understanding systems. Therefore, this trade-off is intolerable for these creative workflows. Given the high copyright value of images in these fields, protection

that ensures robustness against edits without compromising image quality is essential.

On the other hand, zero-watermarking methods [7, 22, 32, 38] offer a compelling alternative by preserving pristine image quality. These methods extract a unique fingerprint or key from the original image and store it externally without altering the image structure. Verification involves checking if a suspect image still possesses this key. While elegant, the robustness of current zero-watermarks is critically low against generative edits. Existing methods [10, 19, 33] primarily rely on fragile high-frequency details, global statistics, or absolute feature descriptors (e.g., from SIFT or deep classifiers), which are precisely what generative models are designed to alter or completely restructure, rendering the watermarks invalid. To address these challenges, we conduct an empirical analysis on images before and after editing. Our findings reveal that, while absolute features and pixel values of an image are drastically altered by generative edits, the **intrinsic relational structure** between partial image regions remains remarkably stable. Specifically, as shown in Fig. 1, we discover that the relative distance between certain pairs of image patches, measured in RGB space, is largely invariant even after complex edits like style transfer or instruction-based manipulation, i.e., if patch i and patch j are “very different” (large RGB distance) in the original image, they tend to remain “very different” after the edit.

Based on this discovery, we propose a novel zero-watermarking framework built upon **Stable Relational Geometry** to extract these invariant patch pairs. Instead of relying on fragile absolute features, our method identifies a unique and resilient set of patch pairs as the zero-watermark, whose relational distance is robustly preserved after substantial editing. Our contributions are as follows:

- We identify and validate a key property for generative editing: the stability of patch-wise relational distance in feature space.
- We propose a novel zero-watermarking framework to learn and predict this stable relational structure from a single image, formulating the watermark as a set of robust patch pairs.
- Experiments demonstrate that our zero-watermarking approach achieves promising robustness against a wide range of generative edits, while inherently maintaining perfect image fidelity.

2. Related Work

2.1. Conventional Embedding Watermarking

Traditional watermarking techniques [1] embed a signal directly into the pixel domain or frequency domain (e.g., DCT, DWT). While effective for simple copyright marking, these methods are fragile and can be easily broken by

geometric transformations, compression, and especially the non-linear reconstruction performed by generative models.

More recently, deep learning-based embedding methods [5, 15, 20, 26, 45] have shown improved performance. They train neural networks to encode messages into images through deep features, and have demonstrated strong robustness against a wide range of distortions (e.g., compression, scaling and noise). In the era of AIGC, to survive diffusion-based AI-editing, several state-of-the-art methods, such as VINE [24] and RobustWide [14], are proposed specifically to withstand these edits. Their strategies involve injecting a powerful, resilient signal into perceptually significant, low-frequency components of the image. However, this introduces an unavoidable trade-off. To achieve robustness against generative models that fundamentally alter pixel data, the embedded signal must be strong, which **inevitably degrades image fidelity**. As a result, such methods are inappropriate for scenarios where preserving pristine visual quality is essential.

2.2. Zero-Watermarking

Zero-watermarking [33] is designed to fundamentally address the fidelity issue. Instead of embedding any signal into the image, it extracts a unique “fingerprint” from the original image and stores it externally (e.g., in a database) alongside the content’s metadata. Verification is then performed by extracting a fingerprint from a suspect image and comparing it to the stored reference. Early methods [10] rely on fragile handcrafted features such as SIFT or SURF. Recent approaches [19, 22, 32, 38] leverage robust deep features from pre-trained networks to achieve improved robustness.

Despite guaranteeing perfect fidelity by design, zero-watermarking exhibits **critically limited robustness** facing modern generative edits. Unlike traditional perturbations, generative models do not simply inject noise. They reconstruct regions, rewrite textures, and modify semantic content. Such transformations fundamentally alter or destroy the absolute feature descriptors and spatial structures that current zero-watermarks rely on. Consequently, existing zero-watermarking techniques fail catastrophically under these modern edits. This exposes a significant gap in the field: the absence of a watermarking paradigm that simultaneously preserves the perfect fidelity of zero-watermarking and delivers the robustness required to withstand generative image manipulation. Our work is designed precisely for it.

3. Pairwise Patch Distance Preservation Under Editing

3.1. Experimental Discovery

We present how the invariance relationship is discovered between patch pairs before and after AI editing. Our experiments demonstrate that, after AI editing, the distance

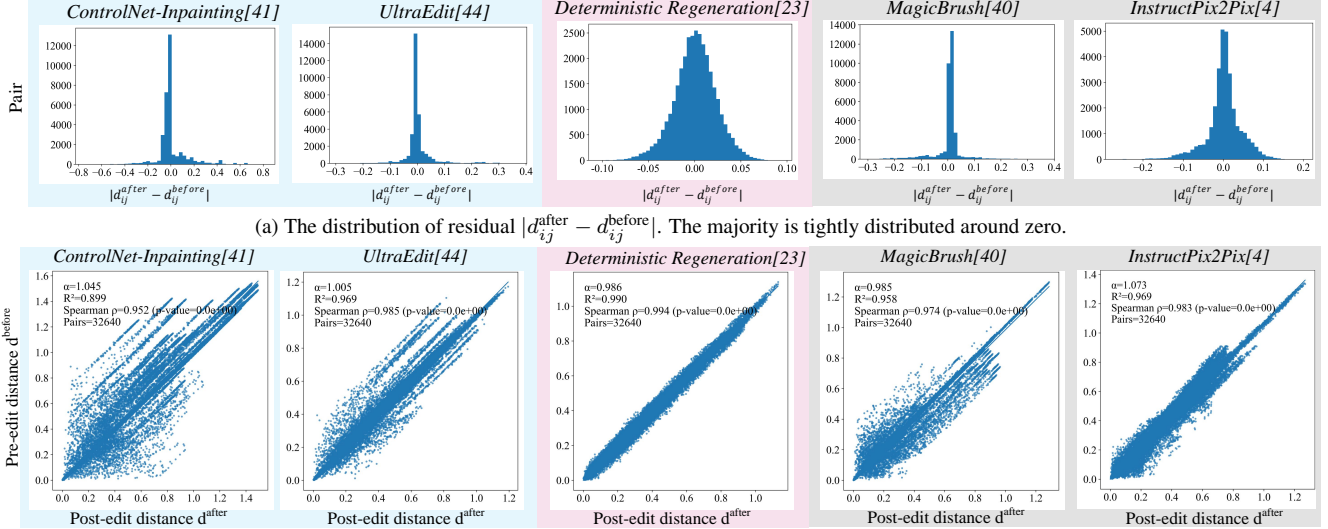


Figure 2. Analysis of Relational Stability.

between corresponding patch pairs remains stable and exhibits a relatively invariant pattern.

Evaluation data: We randomly sample 10,000 instances from UltraEdit [44] and MagicBrush [40] datasets. Of these samples, 2,000 are allocated for deterministic regeneration, another 4,000 for global editing, and 4,000 for local editing.

Pairwise Patch Modeling: We model the images as a set of non-overlapping $N = 256$ patches, represented by their mean RGB vectors $\{v_i\}_{i=1}^N$. The “internal color structure” can be characterized by the $\binom{N}{2}$ pairwise distance in this feature space. Let $d_{ij}^{\text{before}} = \|v_i - v_j\|$ be the L2-distance between the mean RGB vectors of patches i and j in the original image, and $d_{ij}^{\text{after}} = \|v'_i - v'_j\|$ be the distance after editing. Consequently, the difference between the distance before and after editing is defined as $|d_{ij}^{\text{before}} - d_{ij}^{\text{after}}|$.

Key Observation: *The relative distance between particular pairs of patches appears remarkably invariant, even if the edit operation (transformation \mathcal{T}) substantially alters the RGB values of individual patches (mapping v_i to v'_i).*

Experimental Validation: We conduct experiments to analyze distance of RGB vectors before and after three mainstream AI editing methods, including local editing (ControlNet-Inpainting[41], UltraEdit[44]), global editing (InstructPix2Pix[4], MagicBrush[40]) and deterministic regeneration [23]. Fig. 1 depicts the overall variation in patch-pair RGB vectors distance before and after editing and their differences. Furthermore, Fig. 2a illustrates the numerical distribution of these differences.

We observe that the differences exhibit a near-zero-mean, tightly distributed pattern with no evident systematic bias. Besides, the majority of patch-pairs exhibit distance

differences clustered closely around 0.0. These results provide strong evidence that a substantial portion of patch-pair distance remains effectively invariant across the editing process, indicating that intra-image geometric consistency is largely preserved.

To rigorously quantify this phenomenon, we move beyond anecdotal observation and propose a formal geometric hypothesis.

Hypothesis: If the editing transformation \mathcal{T} is indeed “structure-preserving,” it should act as a predictable, geometrically simple operation on this set of pairwise distance. The strongest form is that \mathcal{T} induces a **global similarity transformation** on the feature-space manifold. Therefore, we propose a simple and direct hypothesis: *does a global linear relationship exist between the pre-edit and post-edit distance?*

To validate it, we conduct a large-scale distance-distance correlation analysis. For a given edited image, we compute all $\binom{N}{2}$ pairwise distance d_{ij}^{before} and d_{ij}^{after} . We then visualize their relationship by plotting d_{ij}^{after} (y-axis) against d_{ij}^{before} (x-axis) and perform a linear regression:

$$d_{ij}^{\text{after}} \approx \alpha \cdot d_{ij}^{\text{before}} + \beta, \quad (1)$$

where α denotes a global scaling factor (a “stretching” or “shrinking” of the feature space), and β represents a uniform offset.

Fig. 2b provides compelling support for our hypothesis. The fitted slope $\alpha \approx 1$, offset $\beta \approx 0$, together with the high coefficient of determination ($R^2 > 0.95$) and near-perfect Spearman correlation ($\rho \approx 1$) indicate an exceptionally tight linear correlation between d_{ij}^{after} and d_{ij}^{before} .

It demonstrates that most of the variance in post-edit distance can be directly explained by their pre-edit counterparts. More broadly, this phenomenon reveals a near-**affine invariance** in the feature space: the relative distance among partial patches is preserved up to a uniform scale.

3.2. Theoretical Justification

We delve deeper into our observations to explore why this stability exists. This phenomenon can be attributed to two possible properties of generative editing models:

1. **Fidelity Constraints and Regularization:** Generative editing models, especially diffusion models, are not trained in an unconstrained manner. They explicitly or implicitly incorporate “content/structure preservation” losses. These include perceptual losses (LPIPS) [42], reconstruction losses (L_1/L_2 in latent or pixel space), and various consistency regularizers. Such optimization objectives strongly penalize unnecessary perturbations and encourage the model to learn an identity mapping for non-target regions. As a result, the cross-patch relationships (governing shape, layout, and texture ratios) become a core invariant that these models are optimized to preserve.
2. **Low-Dimensionality of the Edit Subspace:** Semantic edits (e.g., “change style”, “make it summer”) typically correspond to low-dimensional directions or sub-manifolds within the model’s latent space z [12]. When such a latent transformation \mathcal{T} (e.g., $z' = \mathcal{T}(z)$) is decoded, it often applies a functionally uniform change across the image statistics. For example, a style change may apply a similar color-space shift or texture basis change to all patches. When this transformation is approximately affine in the feature space ($v'_i \approx Av_i + b$), the difference between two patch features becomes $v'_i - v'_j \approx A(v_i - v_j)$. The magnitude of this difference is scaled ($\|v'_i - v'_j\| \approx \alpha\|v_i - v_j\|$), but the fundamental relationship is preserved and naturally leads to the strong linear predictability in our empirical analysis.

Together, these findings suggest that patch-pair relational stability is an intrinsic signature during semantic editing, a property we can exploit for robust zero-watermarking. Since this relational geometry is stable and scalable invariant, if we can reliably identify these stable pairs, we can construct a zero-watermark based on these pair indices.

4. Methodology

In this section, we introduce the proposed **Relational Zero-Watermarking (Rel-Zero)** framework, a robust zero-watermarking approach that leverages relational invariance among patch-pair distance to resist generative manipulations. As shown in Fig 3, the framework is composed of three key stages: (1) *Stable patch-pair identification* to

identify the ground-truth invariant pairs as zero-watermark targets; (2) *Patch Relational Learning* to build a network to predict these invariant pairs; and (3) *Watermark Generation and Verification*.

4.1. Stable Patch Pair Identification

We first require a set of “ground-truth” stable patch pairs as the training target. Inspired by [43], we observe that the structural impact of diffusion-based generative edits on patch-pair relationships is analogous to that of its Variational Autoencoder (VAE) component, while the latter is substantially more computationally friendly. Therefore, we employ a pre-trained VAE [18] to simulate the essential content-preserving and smoothing properties of generative pipelines.

The goal is to identify patch pairs (i, j) whose feature-space relationships remain stable before and after VAE reconstruction. Given an input image \mathbf{I} , we first pass it through the VAE to obtain a reconstructed version $\hat{\mathbf{I}} = V_{ae}(\mathbf{I})$.

Both the original image \mathbf{I} and the reconstructed $\hat{\mathbf{I}}$ are partitioned into N non-overlapping patches. Each patch set is then fed into a pre-trained Vision Transformer [8] (ViT) ϕ_{vit} to extract high-dimensional patch-level representations:

$$\mathcal{F} = \phi_{vit}(\mathbf{I}), \quad \hat{\mathcal{F}} = \phi_{vit}(\hat{\mathbf{I}}), \quad (2)$$

where $\mathcal{F} = [\mathbf{f}_1, \dots, \mathbf{f}_N]$ and $\hat{\mathcal{F}} = [\hat{\mathbf{f}}_1, \dots, \hat{\mathbf{f}}_N]$ denote the patch-level embeddings. (Further ViT feature analysis in Appendix Sec. E)

For each patch pair (i, j) , we define their feature difference (L2 distance) before and after reconstruction as:

$$d_{ij} = \|\mathbf{f}_i - \mathbf{f}_j\|_2, \quad \hat{d}_{ij} = \|\hat{\mathbf{f}}_i - \hat{\mathbf{f}}_j\|_2. \quad (3)$$

The stability of a relation is then measured by a similarity score:

$$s_{ij} = \exp\left(-|d_{ij} - \hat{d}_{ij}|\right). \quad (4)$$

The top- K pairs (i, j) with the highest similarity scores s_{ij} are chosen as the ground-truth stable set. These pairs constitute the *invariant relations* \mathcal{E}_g , which serve as the ground-truth target for our zero-watermark.

4.2. Patch Relational Learning

To learn the relational structure from the image features, we construct a fully connected set of patch pairs \mathcal{E} from the ViT-extracted patch features. Each pair $(i, j) \in \mathcal{E}$ corresponds to the relation between patch i and j , where $i, j \in \{1, \dots, N\}$.

We employ a simple edge predictor $\Phi(\cdot)$ to estimate a prediction score p_{ij} for each pair:

$$p_{ij} = \Phi(\mathbf{f}_i, \mathbf{f}_j) = \sigma(\psi(\mathbf{f}_i \oplus \mathbf{f}_j \oplus \|\mathbf{f}_i - \mathbf{f}_j\|_2)), \quad (5)$$

where $\sigma(\cdot)$ denotes the sigmoid activation, $\psi(\cdot)$ represents a MLP network, and \oplus indicates concatenation.

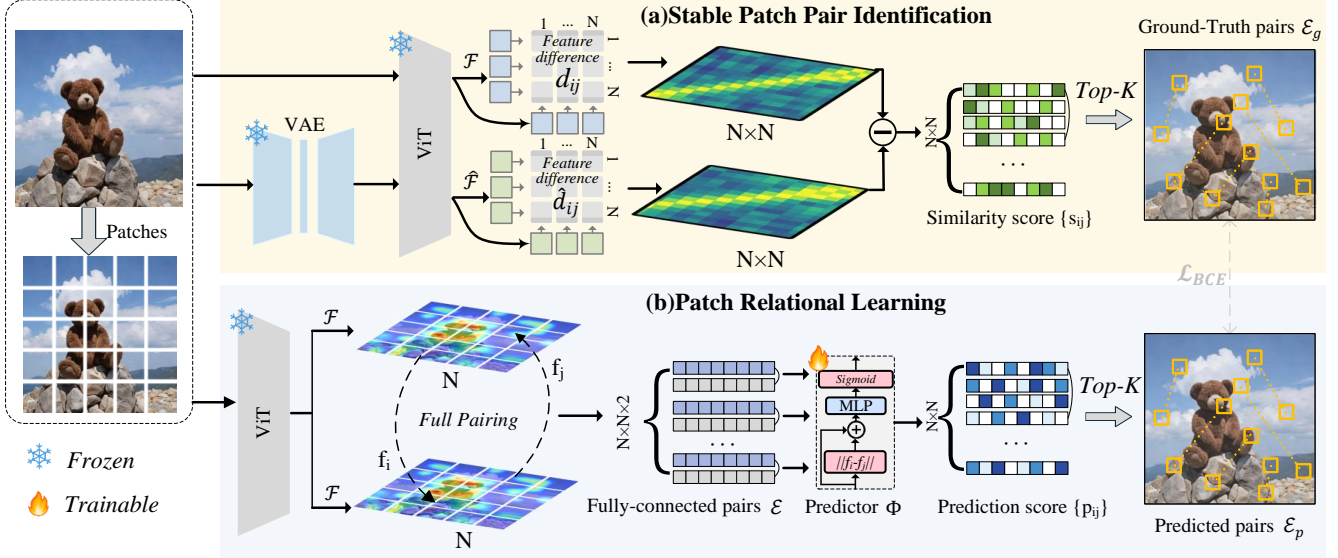


Figure 3. **Framework of the proposed Rel-Zero.** (a) *Stable Patch Pair Identification.* To train a predictor capable of identifying patch pairs with invariant distance relationships, we first construct training targets. A pretrained VAE is employed to simulate generative edits. Features of the original and VAE-modified images are extracted using a ViT to obtain patch-wise features \mathcal{F} and $\hat{\mathcal{F}}$. Pairwise distance is computed on both feature maps, and their differences are measured to identify the most stable top- K pairs surviving edits, which serve as the ground-truth pairs \mathcal{E}_g . (b) *Patch Relational Learning.* Given an input image, ViT features are extracted and all patch pairs are densely formed to construct fully-connected pairs \mathcal{E} . A learnable pair predictor Φ then estimates the stability scores of each pair, which are trained to align with the ground-truth pairs \mathcal{E}_g from (a). During inference (i.e., watermark generation and verification), only the module in (b) is required to generate relational zero-watermarks \mathcal{E}_p .

4.3. Training Objective

The training target aims to align the learned relational scores $\{p_{ij}\}$ with the previously selected invariant pairs. We assign binary labels $y_{ij} = 1$ for the top- K invariant edges and $y_{ij} = 0$ otherwise. The model is trained using the binary cross-entropy (BCE) loss:

$$\mathcal{L}_{BCE} = -\frac{\sum_{i \neq j} [y_{ij} \log(\hat{y}_{ij}) + (1 - y_{ij}) \log(1 - \hat{y}_{ij})]}{N(N-1)}. \quad (6)$$

4.4. Watermark Generation and Verification

Generation. Given an image \mathbf{I} , the relational zero-watermark is defined as the top- K most confident pairs predicted by Φ :

$$\mathcal{E}_p = \text{Top-K}(\Phi(\phi_{\text{vit}}(\mathbf{I}))), \quad (7)$$

where $\mathcal{E}_p = \{(i_1, j_1), \dots, (i_K, j_K)\}$. This index set can be securely stored externally (e.g., hashed or encrypted in a database (detailed in Appendix Sec. B)) without revealing the original content.

Verification. To verify a suspect image \mathbf{I}' , we extract its corresponding pairs:

$$\mathcal{E}'_p = \text{Top-K}(\Phi(\phi_{\text{vit}}(\mathbf{I}'))), \quad (8)$$

and evaluate the similarity score η between \mathcal{E}_p and \mathcal{E}'_p :

$$\eta = \frac{|\mathcal{E}_p \cap \mathcal{E}'_p|}{K}, \quad (9)$$

where $|\cdot|$ denotes set cardinality (i.e., Jaccard-style overlap ratio of edge indices). The image is deemed authenticated at an operating point calibrated for a target false-alarm rate (detailed in Appendix Sec. F).

5. Experiments

5.1. Experimental Setup

Datasets. We conduct our training and evaluation using diverse large-scale image datasets. The network is trained on the COCO[21] dataset. For evaluation, we sample 10,000 instances from the widely-used UltraEdit [44] and MagicBrush [40] datasets as the validation set. Each instance contains a source image, an editing prompt, and a region mask. All images are resized to 224×224 resolution. To ensure a fair and comprehensive evaluation across a diverse range of image content, of these images, 1,000 are allocated for the regeneration task, 1,000 for global editing, 4,000 for local editing, and 4,000 for common degradations.

Baselines. For a thorough evaluation, we compare Rel-Zero to both embedding and zero-watermarking methods. Embedding watermarking includes DWT-DCT[1]



Figure 4. Visualization of pre-edit and post-edit extracted watermarks.

and the recent state-of-the-art VINE [24] and Robust-Wide [14], which are designed against AI editing. For zero-watermarking, since only a few methods are open-sourced, we include ConZWNNet [32] and FGPCET [38], considering their timeliness and representativeness. All baselines are from their officially released checkpoints.

Attack Suite. We subject images to both Generative Editing and common distortions. The implementation details are in Appendix Sec. G.

- **Generative Edit Models.** To comprehensively evaluate robustness, we evaluate against a suite of modern generative editing models. We include InstructPix2Pix [4] and MagicBrush [40] for global editing, UltraEdit [44] and ControlNet-Inpainting [41] for local editing. We also test against deterministic regeneration[23].
- **Common Distortions.** Standard image processing operations including Random Cropout (50% of the area), Scaling (to $0.5\times$ and back), Contrast adjustments $\in [0.5, 2.0]$, Brightness adjustments $\in [0.5, 2.0]$, and Gaussian noise(std = 0.10).

Evaluation Metrics. We evaluate all methods on two

primary axes:

- **Fidelity:** Although zero-watermarking does not affect image fidelity, we introduce PSNR[36], SSIM, and LPIPS[42] to evaluate image quality for a fair assessment between embedding and zero-watermarking methods.
- **Robustness:** To assess watermark survivability, we report the True Positive Rate (TPR) at a highly stringent False Positive Rate (FPR) of 0.1%. This conservative threshold ensures high confidence in the uniqueness of watermark authentication. (detailed in Appendix Sec. F.).

Implementation Details. Unless specified otherwise, we use a patch size of 16×16 , resulting in $N = 196$ patches for a 224×224 image. We use ViT-B/16 [8] as our feature extractor ϕ_{vit} and utilize the VAE from Stable Diffusion v1.4[29]. We set the watermark size to $K = 50$ pairs. Experiments are conducted on an NVIDIA A100 GPU.

5.2. Evaluation Comparison

Fidelity. As shown in Table 1, the major advantage of zero-watermarking over embedding-based watermarking lies in its non-impact on visual quality. Although embedding watermarking methods can achieve reasonably high PSNR and SSIM values, they inevitably introduce slight distortions.

Table 1. Comparison of visual fidelity (PSNR, SSIM, LPIPS) and robustness (TPR@(0.1%FPR)) between Rel-Zero and baseline methods. Zero-watermarking methods do not modify image pixels, thus their PSNR metrics are marked as “-”. Abbreviations: Det (Deterministic Regeneration), Pix2Pix (InstructPix2Pix), Ultra (UltraEdit), CtrlN (ControlNet-Inpainting).

Method	PSNR(dB) [†]	SSIM [†]	LPIPS [↓]	TPR@(0.1%FPR)(%) [†]									
				Regeneration		Global Editing		Local Editing		Common Distortions			
				Det	Pix2Pix	Magic	Ultra	CtrlN	Cropout	Scaling	Contrast	Brightness	Gaussian
Embedding Watermarking													
DWT-DCT [1]	40.38	0.9705	0.0136	0.09	0.04	0.05	0.32	0.56	10.35	6.78	30.18	51.88	12.45
Robust-Wide [14]	41.93	0.9908	0.0034	90.41	97.23	81.97	80.45	82.11	95.31	96.45	98.93	98.89	98.12
VINE [24]	37.34	0.9934	0.0063	99.98	97.46	94.58	99.96	93.04	54.87	76.43	98.43	97.90	98.37
Zero-Watermarking													
ConZWNNet [32]	-	1.000	0.000	0.10	0.02	0.01	5.13	2.41	98.75	97.43	96.22	96.56	98.75
FGPCET [38]	-	1.000	0.000	1.13	0.54	0.11	7.25	3.22	89.31	84.78	86.31	85.44	84.67
Rel-Zero	-	1.000	0.000	85.13	89.65	95.63	96.55	97.43	98.45	98.57	96.45	97.93	95.12

In high-precision domains such as medical imaging, even minor distortions may lead to serious misinterpretations. Therefore, zero-watermarking provides a valuable solution for reliable copyright tracking of high-quality images. (Detailed comparisons in appendix Sec. H.)

Robustness to Generative Edits. Fig. 4 illustrates the watermark extraction results before and after AI editing. Although these editing methods introduce significant structural and visual changes to the images, the difference relationships between certain patch pairs remain preserved, allowing successful watermark extraction. We observe that methods such as InstructPix2Pix and deterministic regeneration showcase larger deviations, this is consistent with our analysis in Fig. 1, where these two methods perform large-scale global edits on images, which are more destructive compared to local editing operations.

Meanwhile, Table 1 reports the robustness of embedding-based and zero-watermarking methods under various AI editing operations. Among embedding approaches, Vine and Robust-Wide exhibit relatively strong performance, largely due to their adversarial training strategies that explicitly incorporate editing models during optimization. However, such strategies incur substantial computational costs, limiting their practicality in resource-efficient or general-purpose settings. In contrast, zero-watermarking baselines rely on invariant feature extraction. Yet these features are heavily distorted or fully overwritten by AI-editing, leading to the failure in watermark detection across diverse manipulation types.

Robustness to common distortions We further evaluate robustness against common image distortions. As shown in Table 1, both zero-watermarking and embedding-based watermarking methods maintain strong performance under conventional perturbations. However, such robustness is typically achieved through extensive adversarial optimization, leading to increased training complexity. In contrast, Rel-Zero naturally maintains high resilience to distortions such as Gaussian noise, scaling, contrast, and brightness

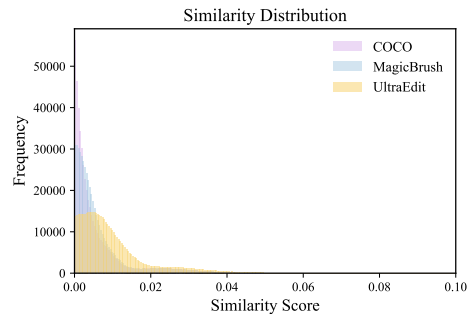


Figure 5. Watermark similarity distribution of different images.

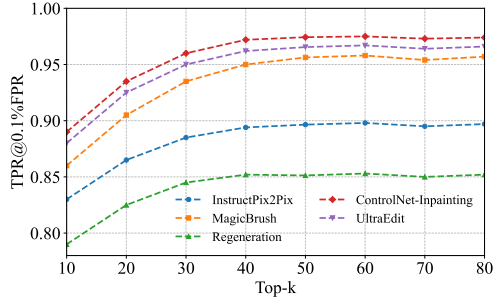
adjustments. These operations introduce largely uniform transformations across the entire image, which may scale patch-pair distance but do not fundamentally alter their relative relationships. As discussed in Sec. 4, this preserves the patch-pair relational geometry, allowing Rel-Zero to maintain high pair-prediction accuracy and enabling stable zero-watermark extraction even under significant degradations. (Additional experiments in Appendix Sec. D.)

5.3. Uniqueness & Collision Analysis

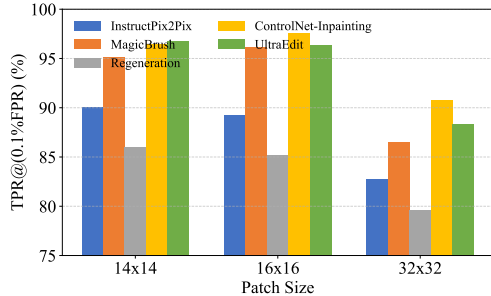
Beyond robustness and fidelity, another essential property of zero-watermarking is **uniqueness** across distinct images. Given two different images $\mathbf{I}_a \neq \mathbf{I}_b$ with their predicted top- K edge sets $\mathcal{E}_p(\mathbf{I}_a)$ and $\mathcal{E}_p(\mathbf{I}_b)$ (Eq. 9), we define their inter-image similarity as

$$\eta_{a,b} = \frac{|\mathcal{E}_p(\mathbf{I}_a) \cap \mathcal{E}_p(\mathbf{I}_b)|}{K}. \quad (10)$$

Ideally $\eta_{a,b} \approx 0$ for $\mathbf{I}_a \neq \mathbf{I}_b$. We quantify it on three datasets—COCO, UltraEdit, and MagicBrush to cover diverse visual domains. For each dataset, we randomly sample 1,000 non-overlapping images, extract \mathcal{E}_p with a fixed $K = 50$, and compute the pairwise similarity $\eta_{a,b}$ among all image pairs. As illustrated in Fig. 5, inter-image similarity remains consistently low across all datasets: most $\eta_{a,b}$ values concentrate near zero with minimal variance, and even



(a) Impact of K (Top- K pairs)



(b) Impact of N (Patch count)

Figure 6. Analysis on the number of top- K pairs and the patch count N . Robustness is evaluated over all edit types.

the rare pairs showing slight correlation exhibit very small magnitudes, effectively ruling out any duplication. These results demonstrate that the learned relational pairs function as *image-specific signatures* rather than generic, content-agnostic templates.

Overall, **Rel-Zero** achieves strong cross-image uniqueness: the overlaps between zero-watermarks from different images are negligible, implying an extremely low probability of ownership collision.

5.4. Parameter Analysis and Ablation Study

We conduct a series of experiments to validate our design choices.

Impact of Top- K . As shown in Fig. 6a, robustness steadily improves as the number of selected top- K pairs grows, but the performance gain saturates beyond $K = 50$. This indicates that the relational redundancy in the watermark is sufficient for stable detection, and incorporating additional pairs yields diminishing returns. Robustness is highest when it comes to ControlNet-Inpainting and UltraEdit, while Regeneration remains the most challenging due to large-scale semantic changes.

Impact of Patch Size. As shown in Fig. 6b, the 14x14 and 16x16 patch sizes yield comparable robustness, as their similar granularity preserves sufficient relational detail. In contrast, performance drops sharply when the patch size increases to 32x32, indicating that overly coarse partitioning

Table 2. Component ablation study. TPR@(0.1%FPR) over ControlNet-Inpainting.

Model Configuration	TPR@(0.1%FPR)
-Ours (ViT + MLP)	97.43
- ViT \rightarrow ResNet-18	84.13
- ViT \rightarrow ResNet-50	85.21
- MLP \rightarrow Transformer+MLP	92.11
- MLP \rightarrow GAT+MLP	94.45

weakens the capacity to model relational structure. The reduced number of patch pairs limits relational redundancy, making the pairing too sparse for the predictor to capture fine-grained semantic invariants.

Component Ablation. To validate our architectural design, we conduct an ablation study on the framework. Specifically, we evaluate the robustness of different architectures under ControlNet-Inpainting. As shown in Table 2, replacing the ViT backbone with either ResNet-18 or ResNet-50 [11] leads to a notable drop in robustness. Although ResNet variants possess strong feature extraction capability, the ViT backbone provides richer low-level priors and captures finer-grained contextual relations, which are more suitable for detecting the relative distance changes between pre- and post-edit patches. Consequently, ViT yields more stable and resilient relational pairs.

On the other hand, we further experiment with adding Transformer or Graph Attention Networks(GAT) [34] layers to the pair predictor. These attention-based designs turn out to provide no extra gains. We hypothesize that the pair prediction task primarily requires accurate estimation of patch-pair distance variations, whereas the attention mechanisms in Transformer or GAT tend to blend patch-wise representations, thereby blurring subtle relational differences and hindering precise distance discrimination.

6. Conclusion

In this work, we uncover a key insight: the relational distance between partial image patches remains remarkably invariant under generative editing. We then introduce Rel-Zero, a relational zero-watermarking framework that leverages this invariant structure to maintain robustness against diverse generative edits without compromising the image quality. Extensive experiments over multiple editing models and distortion scenarios demonstrate that Rel-Zero consistently achieves promising performance in robustness and visual fidelity. We believe this relational invariance provides a promising foundation for reliable provenance tracking in high-fidelity domains and further robust zero-watermarking paradigms in the era of large-scale generative editing models.

Acknowledgements

This work is supported by the National Key Research and Development Program of China under Grant 2024YFE0203200, the Strategic Priority Research Program of the Chinese Academy of Sciences(NO. XDB0690302), the National Nature Science Foundation of China under Grant U24A20329, 62527810 and 62371450.

References

- [1] Ali Al-Haj. Combined dwt-dct digital image watermarking. *Journal of computer science*, 3(9):740–746, 2007. 2, 5, 7, 1
- [2] Eloi Alonso, Adam Jelley, Vincent Micheli, Anssi Kanervisto, Amos J Storkey, Tim Pearce, and François Fleuret. Diffusion for world modeling: Visual details matter in atari. *Advances in Neural Information Processing Systems*, 37: 58757–58791, 2024. 1
- [3] Ashima Anand, Jatin Bedi, Ashutosh Aggarwal, Muhammad Attique Khan, and Imad Rida. Authenticating and securing healthcare records: A deep learning-based zero watermarking approach. *Image and Vision Computing*, 145: 104975, 2024. 1
- [4] Tim Brooks, Aleksander Holynski, and Alexei A Efros. Instructpix2pix: Learning to follow image editing instructions. In *Proceedings of the IEEE/CVF conference on computer vision and pattern recognition*, pages 18392–18402, 2023. 1, 3, 6
- [5] Tu Bui, Shruti Agarwal, and John Collomosse. Trustmark: Universal watermarking for arbitrary resolution images. *arXiv preprint arXiv:2311.18297*, 2023. 1, 2
- [6] Hansheng Chen, Jiatao Gu, Anpei Chen, Wei Tian, Zhuowen Tu, Lingjie Liu, and Hao Su. Single-stage diffusion nerf: A unified approach to 3d generation and reconstruction. In *Proceedings of the IEEE/CVF international conference on computer vision*, pages 2416–2425, 2023. 1
- [7] Pengzhen Chen, Yanwei Liu, Xiaoyan Gu, Enci Liu, Zhuoyi Shang, Xiangyang Ji, and Wu Liu. Plugmark: A plug-in zero-watermarking framework for diffusion models. In *Proceedings of the IEEE/CVF International Conference on Computer Vision*, pages 17335–17345, 2025. 2
- [8] Alexey Dosovitskiy. An image is worth 16x16 words: Transformers for image recognition at scale. *arXiv preprint arXiv:2010.11929*, 2020. 4, 6
- [9] Shenyuan Gao, Jiazhi Yang, Li Chen, Kashyap Chitta, Yihang Qiu, Andreas Geiger, Jun Zhang, and Hongyang Li. Vista: A generalizable driving world model with high fidelity and versatile controllability. *Advances in Neural Information Processing Systems*, 37:91560–91596, 2024. 1
- [10] Baoru Han, Jinglong Du, Yuanyuan Jia, and Huazheng Zhu. Zero-watermarking algorithm for medical image based on vgg19 deep convolution neural network. *Journal of Healthcare Engineering*, 2021(1):5551520, 2021. 2
- [11] Kaiming He, Xiangyu Zhang, Shaoqing Ren, and Jian Sun. Deep residual learning for image recognition. In *Proceedings of the IEEE conference on computer vision and pattern recognition*, pages 770–778, 2016. 8
- [12] Amir Hertz, Ron Mokady, Jay Tenenbaum, Kfir Aberman, Yael Pritch, and Daniel Cohen-Or. Prompt-to-prompt image editing with cross attention control. *arXiv preprint arXiv:2208.01626*, 2022. 4
- [13] Jonathan Ho and Tim Salimans. Classifier-free diffusion guidance. *arXiv preprint arXiv:2207.12598*, 2022. 4
- [14] Runyi Hu, Jie Zhang, Ting Xu, Jiwei Li, and Tianwei Zhang. Robust-wide: Robust watermarking against instruction-driven image editing. In *European Conference on Computer Vision*, pages 20–37. Springer, 2024. 1, 2, 6, 7
- [15] Zhaoyang Jia, Han Fang, and Weiming Zhang. Mbrs: Enhancing robustness of dnn-based watermarking by mini-batch of real and simulated jpeg compression. In *Proceedings of the 29th ACM international conference on multimedia*, pages 41–49, 2021. 1, 2
- [16] K Juluru, JC Shih, A Raj, JP Comunale, H Delaney, ED Greenberg, C Hermann, YB Liu, A Hoelscher, N Al-Khori, et al. Effects of increased image noise on image quality and quantitative interpretation in brain ct perfusion. *American journal of neuroradiology*, 34(8):1506–1512, 2013. 1
- [17] Bahjat Kawar, Shiran Zada, Oran Lang, Omer Tov, Huiwen Chang, Tali Dekel, Inbar Mosseri, and Michal Irani. Imagic: Text-based real image editing with diffusion models. In *Proceedings of the IEEE/CVF conference on computer vision and pattern recognition*, pages 6007–6017, 2023. 1
- [18] Diederik P Kingma and Max Welling. Auto-encoding variational bayes. *arXiv preprint arXiv:1312.6114*, 2013. 4
- [19] Can Li, Hua Sun, Changhong Wang, Sheng Chen, Xi Liu, Yi Zhang, Na Ren, and Deyu Tong. Zwnet: A deep-learning-powered zero-watermarking scheme with high robustness and discriminability for images. *Applied Sciences*, 14(1): 435, 2024. 2
- [20] Jiasen Li, Yanwei Liu, Zhuoyi Shang, Xiaoyan Gu, and Weiping Wang. Drgw: Learning disentangled representations for robust graph watermarking. *arXiv preprint arXiv:2601.13569*, 2026. 2
- [21] Tsung-Yi Lin, Michael Maire, Serge Belongie, James Hays, Pietro Perona, Deva Ramanan, Piotr Dollár, and C Lawrence Zitnick. Microsoft coco: Common objects in context. In *European conference on computer vision*, pages 740–755. Springer, 2014. 5
- [22] Gang Liu, Ruotong Xiang, Jing Liu, Rong Pan, and Ziyi Zhang. An invisible and robust watermarking scheme using convolutional neural networks. *Expert Systems with Applications*, 210:118529, 2022. 2
- [23] Cheng Lu, Yuhao Zhou, Fan Bao, Jianfei Chen, Chongxuan Li, and Jun Zhu. Dpm-solver++: Fast solver for guided sampling of diffusion probabilistic models. *Machine Intelligence Research*, pages 1–22, 2025. 3, 6, 4
- [24] Shilin Lu, Zihan Zhou, Jiayou Lu, Yuanzhi Zhu, and Adams Wai-Kin Kong. Robust watermarking using generative priors against image editing: From benchmarking to advances. *arXiv preprint arXiv:2410.18775*, 2024. 1, 2, 6, 7
- [25] Rui Ma, Mengxi Guo, Yi Hou, Fan Yang, Yuan Li, Huizhu Jia, and Xiaodong Xie. Towards blind watermarking: Combining invertible and non-invertible mechanisms. In *Proceedings of the 30th ACM International Conference on Multimedia*, pages 1532–1542, 2022. 1

- [26] Zhiyuan Ma, Guoli Jia, Biqing Qi, and Bowen Zhou. Safe-sd: Safe and traceable stable diffusion with text prompt trigger for invisible generative watermarking. In *Proceedings of the 32nd ACM International Conference on Multimedia*, pages 7113–7122, 2024. 2
- [27] Mathis Morales and Golnaz Habibi. Synthesizing and identifying noise levels in autonomous vehicle camera radar datasets. *arXiv preprint arXiv:2505.00584*, 2025. 1
- [28] Richard Morin and Mahadevappa Mahesh. Role of noise in medical imaging. *Journal of the American College of Radiology*, 15(9):1309, 2018. 1
- [29] Robin Rombach, Andreas Blattmann, Dominik Lorenz, Patrick Esser, and Björn Ommer. High-resolution image synthesis with latent diffusion models. In *Proceedings of the IEEE/CVF conference on computer vision and pattern recognition*, pages 10684–10695, 2022. 1, 6
- [30] Nataniel Ruiz, Yuanzhen Li, Varun Jampani, Yael Pritch, Michael Rubinstein, and Kfir Aberman. Dreambooth: Fine tuning text-to-image diffusion models for subject-driven generation. In *Proceedings of the IEEE/CVF conference on computer vision and pattern recognition*, pages 22500–22510, 2023. 1
- [31] Mohit Sharma, Ayush Dogra, Bhawna Goyal, Anita Gupta, and Manob Jyoti Saikia. Detail-preserving denoising of ct and mri images via adaptive clustering and non-local means algorithm. *Scientific Reports*, 15(1):23859, 2025. 1
- [32] Deyu Tong, Hongxin Han, Can Li, Fengting Wang, Weilong Kong, and Na Ren. Conzwnet: A contrastive learning-based zero-watermarking network for high robustness and distinguishability. *Journal of Information Security and Applications*, 93:104139, 2025. 2, 6, 7, 1
- [33] Hung-Hsu Tsai, Yen-Shou Lai, and Shih-Che Lo. A zero-watermark scheme with geometrical invariants using svm and pso against geometrical attacks for image protection. *Journal of Systems and Software*, 86(2):335–348, 2013. 2
- [34] Petar Veličković, Guillem Cucurull, Arantxa Casanova, Adriana Romero, Pietro Lio, and Yoshua Bengio. Graph attention networks. *arXiv preprint arXiv:1710.10903*, 2017. 8
- [35] Yiting Wang, Haonan Zhao, Daniel Gummadi, Mehrdad Dianati, Kurt Debattista, and Valentina Donzella. Benchmarking the robustness of panoptic segmentation for automated driving. *arXiv preprint arXiv:2402.15469*, 2024. 1
- [36] Zhou Wang, Alan C Bovik, Hamid R Sheikh, and Eero P Simoncelli. Image quality assessment: from error visibility to structural similarity. *IEEE transactions on image processing*, 13(4):600–612, 2004. 6
- [37] Bin Xia, Yulun Zhang, Shiyin Wang, Yitong Wang, Xinglong Wu, Yapeng Tian, Wenming Yang, and Luc Van Gool. Diffir: Efficient diffusion model for image restoration. In *Proceedings of the IEEE/CVF international conference on computer vision*, pages 13095–13105, 2023. 1
- [38] Hong-ying Yang, Shu-ren Qi, Pan-pan Niu, and Xiang-yang Wang. Color image zero-watermarking based on fast quaternion generic polar complex exponential transform. *Signal Processing: Image Communication*, 82:115747, 2020. 2, 6, 7, 1
- [39] Ning Yu, Vladislav Skripniuk, Sahar Abdelnabi, and Mario Fritz. Artificial fingerprinting for generative models: Rooting deepfake attribution in training data. In *Proceedings of the IEEE/CVF International conference on computer vision*, pages 14448–14457, 2021. 3
- [40] Kai Zhang, Lingbo Mo, Wenhui Chen, Huan Sun, and Yu Su. Magicbrush: A manually annotated dataset for instruction-guided image editing. *Advances in Neural Information Processing Systems*, 36:31428–31449, 2023. 3, 5, 6
- [41] Lvmin Zhang, Anyi Rao, and Maneesh Agrawala. Adding conditional control to text-to-image diffusion models. In *Proceedings of the IEEE/CVF international conference on computer vision*, pages 3836–3847, 2023. 1, 3, 6
- [42] Richard Zhang, Phillip Isola, Alexei A Efros, Eli Shechtman, and Oliver Wang. The unreasonable effectiveness of deep features as a perceptual metric. In *Proceedings of the IEEE conference on computer vision and pattern recognition*, pages 586–595, 2018. 4, 6
- [43] Xuanyu Zhang, Runyi Li, Jiwen Yu, Youmin Xu, Weiqi Li, and Jian Zhang. Editguard: Versatile image watermarking for tamper localization and copyright protection. In *Proceedings of the IEEE/CVF conference on computer vision and pattern recognition*, pages 11964–11974, 2024. 1, 4
- [44] Haozhe Zhao, Xiaojian Shawn Ma, Liang Chen, Shuzheng Si, Rujie Wu, Kaikai An, Peiyu Yu, Minjia Zhang, Qing Li, and Baobao Chang. Ultraedit: Instruction-based fine-grained image editing at scale. *Advances in Neural Information Processing Systems*, 37:3058–3093, 2024. 3, 5, 6
- [45] Jiren Zhu, Russell Kaplan, Justin Johnson, and Li Fei-Fei. Hidden: Hiding data with deep networks. In *Proceedings of the European conference on computer vision (ECCV)*, pages 657–672, 2018. 1, 2

Rel-Zero: Harnessing Patch-Pair Invariance for Robust Zero-Watermarking Against AI Editing

Supplementary Material

A. PCA Analysis Between Generative Editing and VAE

ViT Feature Visualization. We conduct a PCA analysis to visualize how ViT patch embeddings change after two types of transformations: (1) generative editing including ControlNet-Inpainting, UltraEdit, Deterministic Regeneration, MagicBrush, and InstructPix2Pix and (2) Stable Diffusion VAE reconstruction. For each image, we extract patch embeddings before transformation and after either editing or VAE. All embeddings are projected onto the top principal components, and we plot the movement of each patch in this low-dimensional space.

The results show a clear pattern: the global displacement of ViT features induced by VAE reconstruction closely resembles the displacement caused by generative editing. In both cases, only a small subset of patches—typically those corresponding to drastically semantically modified regions—exhibits noticeable shifts, while the majority of background patches remain tightly clustered and nearly unchanged. Moreover, the direction and magnitude of patch movements follow similar trajectories for Edit and VAE.

This strong resemblance indicates that VAE reconstruction preserves the structural behavior of ViT embeddings under real generative edits, despite being a much simpler and deterministic transformation. Therefore, using VAE-induced feature perturbations as a surrogate for analyzing edit-induced changes is both meaningful and well-justified.

B. External Storage Encryption of Relational Zero-Watermark

To protect the relational zero-watermark \mathcal{E}_p , which contains only patch-pair indices but may still leak structural information, we apply a key-controlled permutation encryption. The index set is first converted into a binary indicator vector $\mathbf{b} \in \{0, 1\}^M$, where $M = \binom{P}{2}$. Reshaping \mathbf{b} into an $N \times N$ grid ($N^2 = M$) produces a two-dimensional watermark map suitable for keyed permutation.

We use a secret-key Arnold transform to scramble the spatial layout. Each coordinate (x, y) in the map is permuted to (x', y') according to:

$$\begin{pmatrix} x' \\ y' \end{pmatrix} = \begin{pmatrix} 1 & p \\ q & 1 \end{pmatrix} \begin{pmatrix} x \\ y \end{pmatrix} \pmod{N}, \quad (1)$$

where (p, q, N) jointly define the secret key K . Repeating this transform for T iterations yields the final encrypted wa-

termark:

$$\mathbf{Z}_W = \text{Arnold}^T(\mathbf{b}; K). \quad (2)$$

The encrypted \mathbf{Z}_W does not reveal the patch relations or the underlying image content, and cannot be inverted without the secret key. It can thus be safely stored externally (e.g., hashed or registered in a protected database) and later decrypted using the same key during verification.

C. Time and Memory Cost

Our method further benefits from high computational efficiency. Embedding-based watermarking typically requires running generative models or diffusion sampling during embedding or extraction, resulting in large runtime and memory overhead. Existing zero-watermarking methods also involve heavy CNN backbones or reconstruction modules.

A detailed comparison is shown in Table 1. Rel-Zero avoids these costs entirely. All operations of patch embedding and relational comparison are implemented as a single feed-forward pass with lightweight tensor broadcasts. Consequently, Rel-Zero achieves a total extraction time of **0.3 ms** and a memory cost of only **0.3 GB**, outperforming prior zero-watermarking approaches by an order of magnitude and embedding-based schemes by more than two orders of magnitude.

Table 1. Runtime and memory comparison. “Total Time” measures end-to-end watermark extraction per image (or embedding+extraction for embedding-based methods). CPU-only implementations (e.g., DWT-DCT and FGPCET) report no GPU memory usage and are omitted for fairness.

Method	Total Time (s)	Memory (GB)
DWT-DCT [1]	–	–
Robust-Wide [14]	0.0268	3.1
VINE [24]	0.0674	5.2
ConZWNNet [32]	0.0013	2.3
FGPCET [38]	-	-
Rel-Zero (Ours)	0.0003	1.5

D. Additional Robustness Experiments

To further evaluate the stability of relational cues under low-level corruptions, we compare Rel-Zero and baseline methods under three categories of common distortions: (1) **Salt&Pepper noise**, applied with corruption probabilities $p=0.01$ and $p=0.03$; (2) **JPEG compression**, evaluated

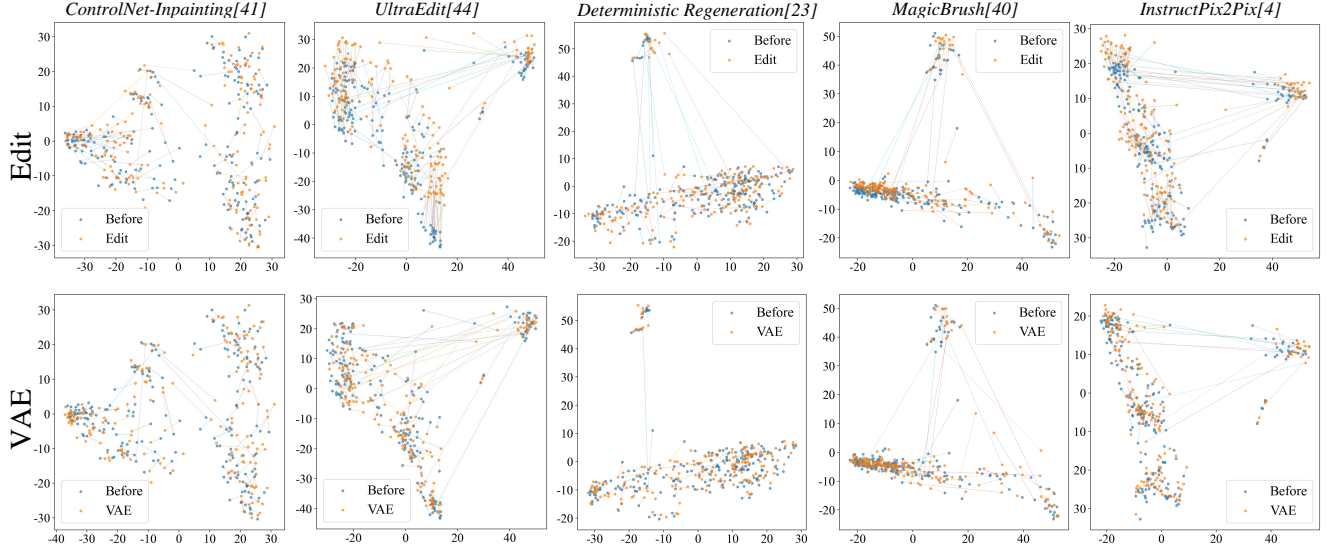


Figure 1. PCA visualization of ViT patch embeddings before and after generative editing or VAE reconstruction. Both transformations cause similar displacement patterns: only patches in drastically semantically edited regions move noticeably, while most patches remain stable. The similarity of these trajectories demonstrates that VAE reconstruction effectively mimics edit-induced feature changes.

Table 2. Robustness under common distortions measured by TPR@(0.1%FPR). We report results under Salt&Pepper noise, JPEG compression, and small-angle rotation.

Method	Salt & Pepper		JPEG		Rotation	
	S&P-1	S&P-2	Q = 90	Q = 50	Rot-3°	Rot-5°
Embedding Watermarking						
DWT-DCT [1]	85.56	80.21	68.53	70.21	0.02	0.05
Robust-Wide [14]	98.89	98.55	93.55	95.76	2.43	3.56
VINE [24]	100.00	100.00	99.45	99.56	5.43	6.78
Zero Watermarking						
ConZWNNet [32]	99.11	99.59	98.56	99.28	98.13	96.45
FGPCET [38]	99.06	98.65	98.79	99.19	99.98	99.66
Rel-Zero	100.00	99.86	98.28	99.00	95.54	90.21

at quality factors $Q=90$ (mild compression) and $Q=50$ (strong compression); and (3) **Rotation**, using angle perturbations of 3° and 5° . All distortions are applied directly to the input image without any pre-alignment or post-processing.

Across all distortion types and strengths, Rel-Zero consistently maintains high robustness. These results confirm that relational differences between patch pairs remain highly stable even under pixel-level perturbations, and that the relational design provides strong inherent robustness without requiring additional denoising, error correction, or adversarial training.

E. ViT Embedding Stability Under Generative Editing

The core premise of our method is that modern generative editing models (InstructPix2Pix, UltraEdit, etc.) tend to preserve the *relational geometry* of deep features, even when the edited image exhibits large visual or semantic changes. In this section, we provide additional evidence showing that the **pairwise relationships between ViT patch features remain stable** after editing, analogous to the relational behavior previously observed in RGB vectors. This structural stability directly justifies our use of patch-pair distance of ViT features as reliable watermark carriers.

Self-Similarity Matrix (SSM) Stability for ViT Features. Given a ViT feature map $F = \{f_i\}_{i=1}^N$ extracted from an image, we compute the self-similarity matrix:

$$M(i, j) = \|f_i - f_j\|_2.$$

Figure 3 visualizes M_{before} and M_{after} for the same image before and after generative editing. Despite significant local modifications (e.g., object replacement or style alteration), the global structure of M remains nearly unchanged, up to a global scaling factor α that we estimate via linear regression. The residual matrix

$$|M_{\text{after}} - M_{\text{before}}|$$

remains close to zero across most regions, demonstrating that *the intrinsic geometric layout of patch features is preserved*. This mirrors the behavior previously observed in

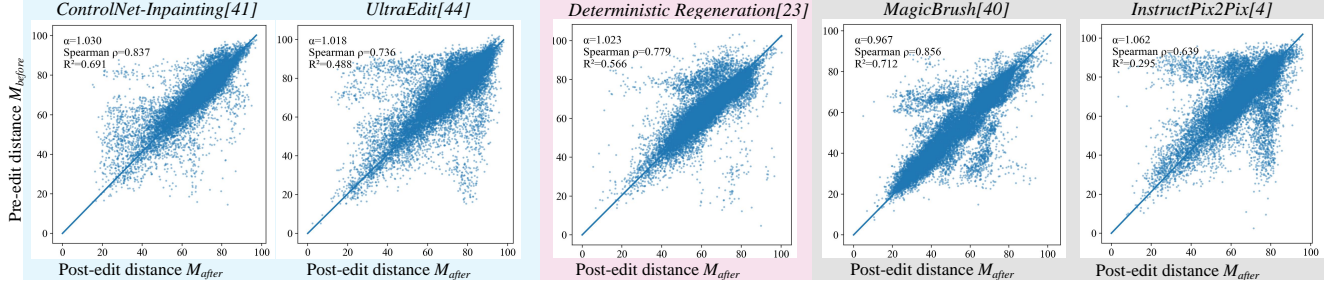


Figure 2. **Correlation between patch-pair ViT features distance before and after editing.** Distance aligns strongly with a fitted linear model $M_{\text{after}} \approx \alpha M_{\text{before}}$, confirming that ViT patch-pair relationships remain stable and support our relational watermark extraction.

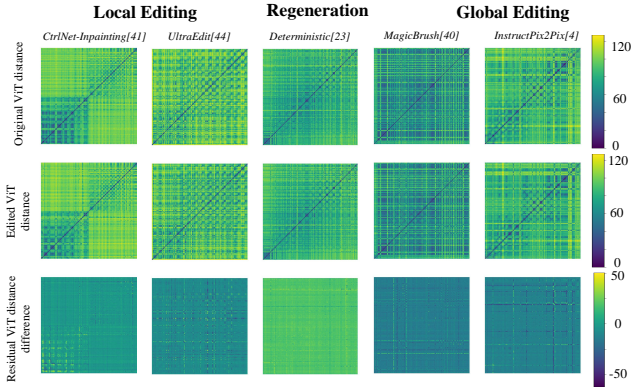


Figure 3. **ViT Self-Similarity Matrix stability under editing.** First row: SSM before editing. Second row: SSM after editing. Right: Residual $|M_{\text{after}} - M_{\text{before}}|$. The near-zero residual indicates that the relational geometry of ViT patch features is preserved up to a global scale.

pixel-space (RGB) self-similarity patterns, but the effect is more pronounced in deep representations due to their semantic stability.

Patch-Pair Distance Correlation. To quantify the consistency of feature geometry, we also plot the pairwise condensed distance $M(i, j) = \|f_i - f_j\|_2$ before and after editing in a scatter diagram (Figure 2). The majority of the scatter points lie tightly along a line

$$M_{\text{after}} \approx \alpha M_{\text{before}},$$

achieving high Pearson correlation and high coefficient of determination. This strong linear relationship indicates that editing operations largely preserve the *relative* differences between patch features, even if absolute feature values shift.

Implications for Relational Watermarking. Together, the SSM visualizations and distance-correlation scatter-plots demonstrate that ViT feature geometry is **stable under a wide range of generative edits**, same as the RGB vectors in Sec 3.1. Since our watermark is based on the ordering and relationships of patch-pair distances, and these relationships remain invariant up to scale, the feature relational

structure survives editing. These results provide strong empirical support for the theoretical basis of Rel-Zero and explain why our method remains robust across global and local edits.

F. TPR with a Fixed FPR

We treat all embedding-based watermarking methods as single-bit schemes, with an embedded watermark $s \in \{0, 1\}^k$. A predefined threshold $\tau \in [0, k]$, is used for detection. If the similarity score $\text{Acc}(s, s')$ between the original watermark s and the extracted one s' surpasses or equals τ , the image is deemed as watermarked.

According to prior work [39], it is generally assumed that the extracted bits s'_1, \dots, s'_k from unmarked images follow an independent and identically distributed Bernoulli process with success probability 0.5. Under this assumption, the similarity metric $\text{Acc}(s, s')$ conforms to a binomial distribution with parameters $(k, 0.5)$.

Once this distribution is known, the false positive rate (FPR) corresponds to the likelihood that a non-watermarked image still achieves a score above the threshold τ . This can be formally represented using the regularized incomplete beta function $B_x(a, b)$ as follows:

$$\begin{aligned} \text{FPR}(\tau) &= P(\text{Acc}(s, s') > \tau) = \sum_{i=\tau+1}^k \binom{k}{i} \left(\frac{1}{2}\right)^k \\ &= B_{1/2}(\tau + 1, k - \tau). \end{aligned} \quad (3)$$

For zero-watermarking method, we treat our relational watermarking scheme as a binary detection problem, where a fixed relational index set \mathcal{E}_p (consisting of K patch-pair edges) serves as the watermark signature. During verification, the detector extracts a candidate edge set \mathcal{E}'_p from the query image and computes the similarity score

$$\eta = \frac{|\mathcal{E}_p \cap \mathcal{E}'_p|}{K}. \quad (4)$$

A detection threshold $\tau \in [0, 1]$ is predetermined, and the image is deemed watermarked if the overlap ratio η reaches or exceeds this threshold.

Following common practice in watermark detection, we model the prediction of watermark edges from clean (unrelated) images as random and independent activations. That is, each true watermark edge in \mathcal{E}_p is falsely activated with a small probability 0.5, and the K detection outcomes are assumed to follow a binomial distribution with parameters $(K, 0.5)$.

Once this distribution is established, the false positive rate (FPR) corresponds to the probability that a clean image still produces an overlap ratio above the threshold τ :

$$\text{FPR}(\tau) = P(\eta \geq \tau) = P(X \geq \tau K) = \sum_{i=\lceil \tau K \rceil}^K \binom{K}{i} p^i (1-p)^{K-i}. \quad (5)$$

In our evaluation, we maintain the FPR at 0.1% to determine the corresponding operating threshold τ , and subsequently report the true positive rate (TPR) computed over 1,000 watermarked images. As shown in Table 1, at a fixed FPR of 10^{-3} our relational watermarking method achieves strong TPR and reliable detection performance.

G. AI-Editing Setting

For deterministic regeneration, we employ the fast sampler DPM-Solver [23] and evaluate with a sampling step setting of $n_d = 25$.

We use each model’s default sampler and perform 50 sampling steps to generate edited images. For global editing, the difficulty level is controlled by the classifier-free guidance scale of the text prompt [13], which we set to 8, while fixing the image guidance scale to 1.5. For local editing, difficulty is determined by the ratio of the edited region to the entire image, controlled through the region mask size with intervals of 10–20%, 20–30%, 30–40%, 40–50%, and 50–60%. Across all local editing settings, the image and text guidance scales are fixed at 1.5 and 7.5, respectively.

H. Visual Comparison of Embedding-Based and Zero-Watermarking Methods

To qualitatively assess the perceptual impact of different watermarking paradigms, we provide a visual comparison consisting of the original image, the embedding-based watermarked image, its corresponding residues, and the visualization of zero-watermarking methods (Fig. 4).

Embedding-based watermarking inevitably introduces pixel-level perturbations to encode information. Although these perturbations may appear imperceptible in the watermarked image, they accumulate into clear artifacts in the residue map, revealing the underlying distortion injected into the visual content.

In contrast, our zero-watermarking approach requires *no* modification to the input image. The extracted relational structure is purely feature-driven and leaves the pixel

space entirely untouched. Consequently, it produces no observable residue, highlighting the key advantage of zero-watermarking: robust verification without introducing any noise or degradation to the perceptual quality.

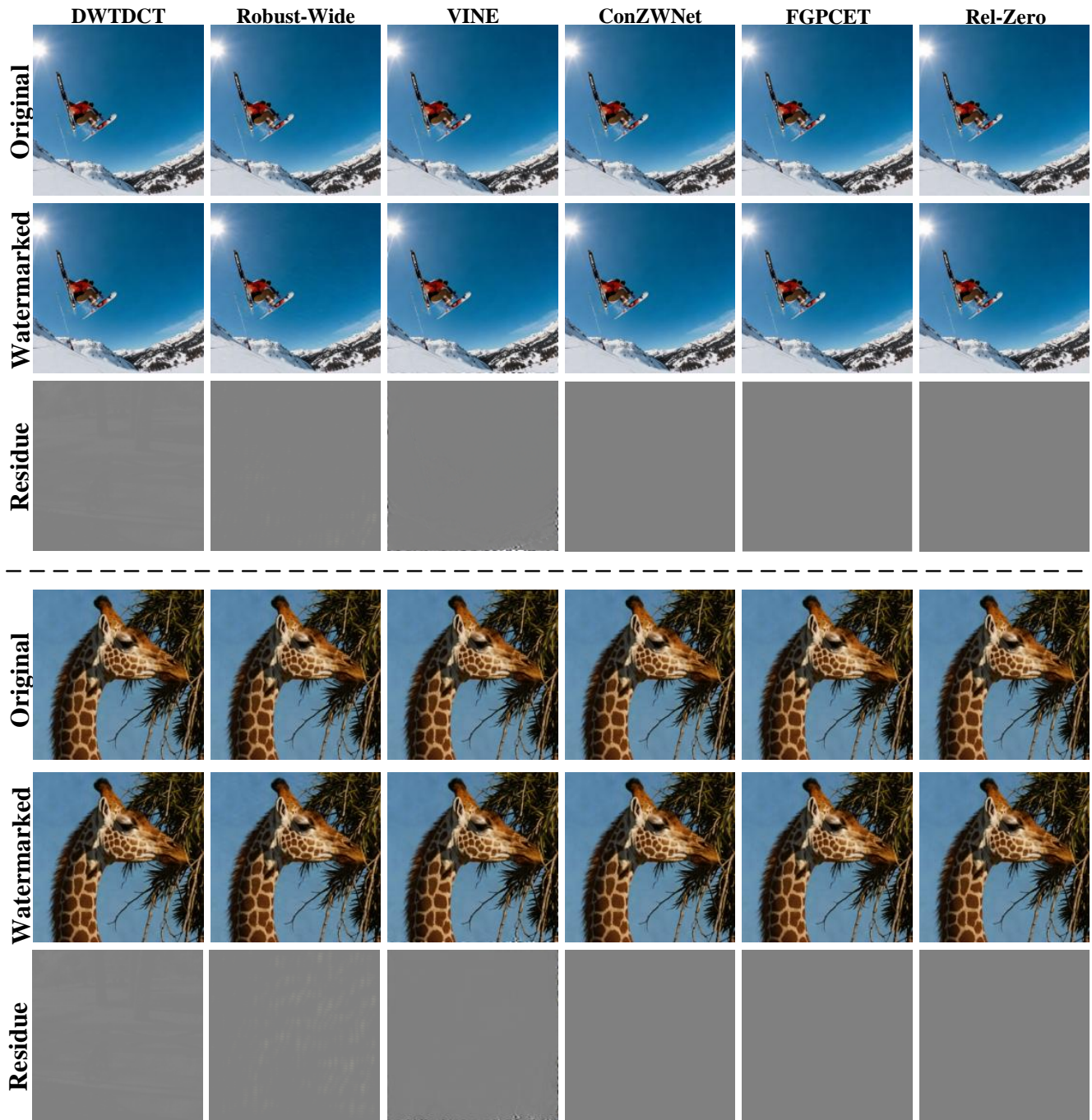


Figure 4. **Visual comparison of embedding-based watermarking and zero-watermarking.** From left to right: original image, embedding-based watermarked image, residue highlighting injected perturbations, and our zero-watermarking visualization. Unlike embedding-based methods, zero-watermarking introduces *no pixel-level noise*, preserving perfect perceptual fidelity. Zoom in to see the detailed difference.